



Assessment of the 2015 full-scale ten-story RC test Structure using ASCE/SEI 41

Kristijan Koložvari¹ · Saman Abdullah^{2,4} · John Wallace² · Koichi Kajiwara³

Received: 30 November 2022 / Accepted: 19 February 2023 / Published online: 4 March 2023
© The Author(s), under exclusive licence to Springer Nature B.V. 2023

Abstract

This paper presents application of ASCE/SEI 41–17 nonlinear seismic analysis and evaluation procedures to the 10-story reinforced concrete building tested on the E-Defense shake table in December 2015. Primary lateral load resisting system of the building was reinforced concrete frame in the longitudinal direction and RC wall in the transverse direction. Analytical models were developed in OpenSees with nonlinear wall, beam, and column elements, as well as with linear elastic and two types of nonlinear beam-column joint elements: (1) modeling parameters that follow ASCE/SEI 41–17 recommendations, and (2) modeling parameters derived using data from relevant experimental results. Computed responses for the analytical models of the building and predicted damage are compared with measured responses and observed damage for strong motion records from 50 and 100% Kobe earthquake excitations. Results comparisons indicate that the ASCE/SEI 41–17 nonlinear dynamic evaluation procedures are overall able to reasonably identify the general damage extent and distribution for both frame and wall directions. Analysis results further suggest that the beam-column joint modeling parameters in ASCE/SEI 41–17 for nonlinear dynamic procedures likely overestimate the rate of strength loss with increasing deformation demands revealing a potential need for review and update of the joint shear strength and nonlinear modeling parameters and acceptance criteria.

Keywords 10-story RC E-Defense test structure · SEI/ASCE-41 · Nonlinear dynamic analysis · Reinforced concrete buildings · OpenSees

✉ Kristijan Koložvari
kkoložvari@fullerton.edu

¹ California State University, Fullerton, USA

² University of California, Los Angeles, USA

³ NIED, Miki, Japan

⁴ University of Sulaimani, Sulaymaniyah, Iraq

1 Introduction

Building design and evaluation methodologies that target a desired seismic performance (performance-based seismic design) have been widely applied in recent years to new and existing reinforced concrete (RC) buildings. The performance-based design approach heavily relies on results of nonlinear response history analyses of complete three-dimensional building models to obtain engineering demand parameters that are compared with a set of acceptance criteria to judge if the structural response is acceptable. ASCE/SEI 41–17 (ASCE 2017) is the most commonly used standard in the United States for seismic evaluation and retrofit of existing buildings. The objective of the seismic evaluation provisions described in ASCE/SEI 41–17 is to evaluate deficiencies that prevent a building from achieving a selected Performance Objective. Previous work assessed new RC buildings designed according to ASCE/SEI 7, using ASCE/SEI 41 and identified relative inconsistencies between the two standards; specifically, structures designed in accordance with ASCE/SEI 7 may not “pass” a linear, and in some cases a nonlinear evaluation in accordance with ASCE/SEI 41 evaluation (Sattar 2018; Buniya et al. 2017). However, these findings are limited to the study of code-compliant buildings that typically would be considered “benchmark” buildings and deemed to comply with ASCE/SEI 41 due to their incorporation of prescriptive ductile detailing and minimum strength requirements.

As identified by a workshop conducted in 2008 (NIST 2009), there is a need to systematically benchmark the primary outcomes of the evaluation process and determine how well ASCE/SEI 41 represents actual damage that could occur due to strong shaking. This is particularly relevant with the structural engineering profession moving towards risk assessment of buildings that relies on accurate estimation of damage across a wide range of shaking intensities. Seismic retrofit of existing non-ductile concrete structures tends to require measures that have a significant environmental impact due to the carbon-intensive nature of the new structural elements. In order to minimize these impacts, accurate damage assessment methodologies are required to ensure that only the buildings requiring retrofit are identified and that the retrofit scope is highly efficient.

In 2016, the Applied Technology Council (ATC), with funding from National Institute of Standards and Technology (NIST), commenced the ATC-134 project to benchmark evaluation procedures in ASCE/SEI 41 with respect to data recorded for eight RC structures subjected to actual earthquakes or tested on a shake table. Results reported in this paper are a part of this effort.

The primary objective of this paper is to benchmark evaluation methodologies for existing RC buildings and present recommendations for improvement of the seismic evaluation procedures of ASCE/SEI 41–17 (ASCE 2017). For this purpose, calculated results from implementing evaluation procedures described in applicable methodologies (ASCE/SEI 41) are compared to test data available for a 10-story RC building tested on the E-Defense shake table in December 2015 in Japan (Nagae et al. 2015). Analyses were conducted in accordance with the Nonlinear Dynamic Procedures described of ASCE/SEI 41–17 using OpenSees (McKenna et al., 2011). Analytical results were compared to observed performance of the structure through component and global response and overall damage distribution in the building. Based on the findings, recommendations are made for improvements to ASCE/SEI 41 procedures. This paper presents a selected set of results obtained for this study. Additional information can be found in NIST report (NIST 2022).

2 Brief description of experimental program

2.1 Building description

2.1.1 Geometry and structural system

The structure evaluated in this paper was cast-in-place RC with mild reinforcement tested in December 2015 on the E-Defense shake table. The 10-story test specimen was 27.4 m tall, and plan dimensions were 9.7 m × 15.7 m at the first floor and 9.5 m × 13.5 m at the other floors. The lateral force-resisting system of the building consists of two lines of perimeter moment frames in the longitudinal direction and four shear walls in the transverse direction that terminate at the top of the 8th floor. There also are two lines of interior beams (three beams per line) in the longitudinal direction that frame between the shear walls in the out-of-plane direction, and four lines of beams (two beams per line) in the transverse direction that frame between the perimeter columns and the shear walls in the in-plane direction. The building was structurally regular and was designed to conform to the seismic design provisions of the Architectural Institute of Japan (AIJ 2018) and meet most of the ACI 318–14 provisions for Special Moment Frame and Special Structural Wall systems, as detailed in Unal et al. (2020).

Typical moment frame column sections are 500 mm × 500 mm, and typical beam sections are 350 mm × 500 mm. Both columns and beams are well-confined at member ends. The webs of the shear walls were 150 mm thick at 1st through 7th levels and reduced to 120 mm at the 8th level and above. To allow transportation of the specimen inside the test facility, the structure was built in two separately fabricated sections, where both sections are bolted together at the midpoint of columns and shear walls at the 6th story; therefore, any comparisons between test and model results adjacent to this splice should consider the impact of the presence of the splice. Additional details about the test specimen are presented by Nagae et al. (2015) and NIST (2022).

2.1.2 Material properties

The tested material strengths are given in Table 1 (Unal et al., 2020). For the purpose of this evaluation, the measured (representative or mean) material strengths were used for all elements.

2.1.3 Building weight

The building weighed 9545 kN, which includes the dead load (structural elements) and attached fixtures, such as stairs, steel framing, and instrumentation. Floor weight ranged from 579 to 905 kN for typical floors, except for level 6, where due to the weight of steel fixtures the floor weight was 1058 kN, and level 1, which also included the weight of the foundation resulting in total floor weight of 1856 kN. Weight was assumed to be evenly distributed across the slab.

Table 1 Material Properties Based on Test Results (Mean values)

Floor	Height (m)	(a) Concrete		(b) Reinforcement			f_y (MPa)	f_u (MPa)	E_s (GPa)
		Wall	Beam	Column	E_c (MPa)	Bar No. Beams and columns longitudinal reinforcement			
R	–	–	27	–	–	D22 (SD345)	389	574	189
10	2.5	27	27	27	30400	D19 (SD345)	388	582	190
9	2.5	27	27	27	32448	Wall longitudinal bars			
8	2.5	27	27	27	32882	D13 (295A)	361	498	197
7	2.55	27	27	27	32613	Transverse reinforcement			
6	2.55	27	33	27	34475	D10 (295A)	408	536	197
5	2.55	33	33	33	30104	D13 (295A)	361	498	197
4	2.6	33	33	33	30159	S10 (1) (KSS785)	900	1049	206
3	2.6	33	42	33	33758	S10(3) (KSS785)	962	1153	204
2	2.6	42	42	42	36847	Slab reinforcement			
1	2.8	42	42	42	35137	D10 (295A)	353	495	186

2.1.4 Instrumentation

Specimen instrumentation included 654 channels to record responses that included story displacements, floor accelerations, joint deformations, beam and column end rotations, and wall average shear and vertical strains (Sato et al. 2017). Floor accelerations were measured using two triaxial accelerometers attached to the floor slabs at north-east and south-west corners. Story displacements were measured using displacement transducers attached to steel frames at every floor level. Wall vertical strains were measured using LVDTs attached to wall boundaries over the first three stories. To measure member-end rotations, displacement transducers were installed along beam and column hinging regions.

2.1.5 Ground motions and testing protocol

The ground motions recorded at JMA's Kobe station (referred to as Kobe ground motion in further text) were used as the input excitation for the test building. The maximum accelerations for the north–south (NS), east–west (EW), and up–down (UD) directions are 8.18 m/s², 6.17 m/s², and 3.32 m/s², respectively. The NS component of the ground motion was applied in the frame direction, whereas the EW component was applied in the wall direction. The test was carried out in two phases. In phase 1, the building sits on eight flat-plate friction sliders allowing the building to dissipate energy, whereas in phase 2, the building is bolted to the shake table to provide a fixed restraint support condition. Ground motions were scaled by 10%, 25%, 50%, and 100% and applied sequentially in the two phases of testing. White noise excitation was applied before and after each individual ground motion to estimate the first mode period of the structure.

Table 2 Test and Model Fundamental Periods

Structure base test condition	Structure base test condition	Building period after application of ground motion (seconds)			
		Test		OpenSees model	
		Frame Dir	Wall Dir	Frame Dir	Wall Dir
Sliding base	Initial	0.57	0.57	0.67	0.43
	10%	0.61	0.61	–	–
	25%	0.69	0.63	–	–
	50%	0.76	0.64	–	–
	100%	0.87	0.69	–	–
Fixed base	Initial	0.85	0.58	–	–
	10%	0.87	0.58	–	–
	25%	0.94	0.6	–	–
	50%	1.24	0.74	–	–
	100%	2.43	1.13	1.41	0.72
	60%	2.62	1.19	–	–

2.2 Observed performance

Periods of the test structure after application of each ground motion are reported in Table 2. Initial natural periods of the test structure, as obtained from the white noise test, were 0.57 s in both wall and frame direction. After initial softening in the sliding base tests (0.87 s and 0.69 s for the frame and wall directions, respectively), the natural periods for the frame and wall directions increased slightly (0.85 s and 0.58 s to 0.94 s and 0.60 s for the frame and wall directions, respectively) in the 10% and 25% Kobe fixed-base tests, modestly in the 50% Kobe fixed-base test, and appreciably in the 100% Kobe fixed-base test.

For the fixed-base test and the 100% JMA-Kobe motion, the maximum story drift ratios of 3.05% and 1.50% were measured for the frame and wall directions, respectively. Story drift ratios are largest for the frame direction between the 3rd and 4th story, where damage was concentrated, whereas story drift ratios for the wall direction increase only modestly above the 1st floor due to the rigid body rotation at the wall base due to the concentration of nonlinear curvature at the critical section (wall-foundation interface) and possible (minor) foundation rotation (Garcia, 2020).

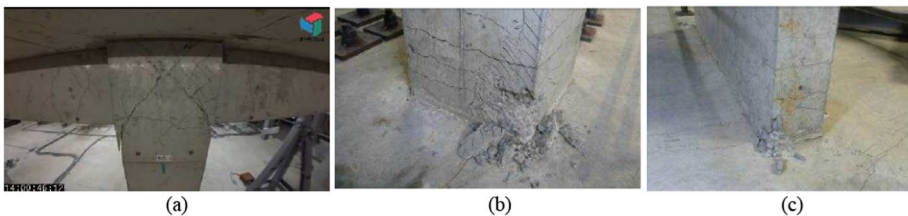


Fig. 1 Photos of observed damage (Tosauchi et al. 2017): **a** beam-column joint at 4th floor, **b** column base at 1st floor, **c** wall boundary element at 1st floor

In terms of damage, under the 100% excitation for the fixed-base test, observations included significant beam-column joint damage characterized by diagonal cracking (e.g., Fig. 1a) at the 3rd, 4th and 5th floors, minor concrete cover spalling at the base of 1st floor corner columns (Fig. 1b) and at the base shear wall (Fig. 1c). Damage to the beam-column joints appeared to produce softening that led to fairly large story drift ratios (3.05%) in the frame direction for the 100% Kobe record (Table 2), whereas damage in the wall direction was minor. More information on the test procedure, specimen design, instrumentation, and experimental results for the 2015 tests can be found in Kajiwara et al. (2015), Sato et al. (2017), and Tosauchi et al. (2017).

3 Description of the nonlinear modeling approach

3.1 General

Three-dimensional nonlinear OpenSees models were developed following ASCE/SEI 41–17 standard. The structure was modeled with a fixed-base and semi-rigid diaphragms using shell elements (Fig. 2). For the fiber section models, columns and beams were discretized using several displacement-based fiber section elements along the length of the members, each element with three integration points and Legendre integration, whereas walls were modeled with a three-dimensional multiple-vertical-line-element model (MVLEM-3D; Kolozvari et al 2021) with nonlinear in-plane behavior and elastic out-of-plane behavior. More details about the model description and calculation of modeling parameters are provided in the following section as well as in the NIST report (NIST 2022).

Masses and gravity load at each level were based on values reported by Nagae et al. (2015). For gravity load, self-weight (excluding the slab) was accounted for with a line load applied along the length of beams and columns, whereas the remaining gravity load

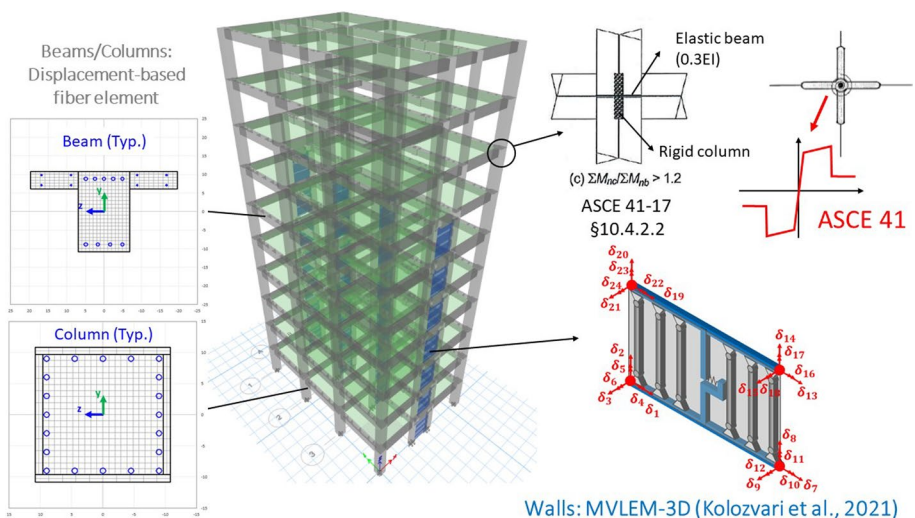


Fig. 2 General element modeling approaches

was distributed on the slab. Masses were distributed to nodes at each floor level based on the distribution of gravity load. No load factors were applied to the gravity loads.

3.2 Component modeling

Nonlinear fiber section modeling was used for beams, columns, and walls, whereas two approaches were used to model the beam-column joints, one with elastic joints (EJ) and the other with nonlinear joints (NJ). Since preliminary assessment of the building design indicated high potential for joints nonlinear behavior (Unal et al., 2020), results obtained with elastic joints model are not considered to be as relevant as the results obtained using the model with nonlinear joints and are reported as part of the sensitivity studies (Sect. 5). All columns and beam were expected to respond primarily in a flexure mode because they had relatively significant confinement, such that their shear strength exceeded, by a significant margin, the shear demand associated with flexural yielding. Therefore, the gross elastic shear stiffness was used for the frame members, as recommended by ASCE/SEI 41–17. Effective flange width of beams, determined based on ASCE/SEI 41–17 Sect. 10.3.1.3, was considered in strength and stiffness of the beams. A biaxial mesh was used to model beams and columns, as shown in Fig. 2.

Beam-column joints were classified as “conforming” per ASCE/SEI 41–17 despite the relatively wide transverse reinforcement spacing (150 mm) in the joint. Demand-to-capacity ratios for beam-column joints computed according to ACI 318–14 between Levels 2 and 7 were determined to range from 0.40 to 0.52 for exterior connections and 0.54 to 0.65, respectively (Unal et al., 2020). In the OpenSees EJ model, beam-column joints were modeled using elastic elements extending from the beam-joint and column-joint interfaces and connecting at the center of the joint. Since the ratio of the summation of the column nominal moment capacities ($\sum M_{nc}$) to the summation of the beam nominal moment capacities ($\sum M_{nb}$) of each joint was greater than 1.2, joint elastic stiffness was modeled implicitly according to ASCE/SEI 41–17 Sect. 10.4.2.2 (option “c” from Fig. 10-2 of ASCE/SEI 41–17), as shown in Fig. 2, in the OpenSees EJ model. In the OpenSees NJ models (Fig. 3), joints were modeled using the “scissor model” as described by Celik and Ellingwood (2008), where joint elastic elements extended from beams and columns and rotational springs were introduced in the frame direction, to allow a scissor motion in the joint (Fig. 2). Capacities of the beam-column joints were obtained using the joint shear strength equation per ACI 318–14 and were therefore different for the interior and exterior bays. It should be noted that neither the scissor model nor the ACI joint shear strength equation consider variation of beam-column joint shear strength due to varying axial load during the earthquake motion. The stiffness of the elastic elements and the nonlinear behavior of the rotational springs was calibrated using two options. Option 1 (Fig. 3a): the stiffness of elastic beam/column elements framing into the joint was modeled according to ASCE/SEI 41–17 Sect. 10.4.2.2, as described above, while joint nonlinear behavior is as defined in ASCE/SEI 41–17 Sect. 10.4.2 and Table 10–11. For this option, results from pushover analysis indicated that including slip spring in the joint model had minor impact; therefore, slip springs are ignored. Option 2 (Fig. 3b): the stiffness of elastic beam/column elements framing into the joint was assumed to be rigid per “explicit joint model” described in Fig. 10-2(a) of ASCE/SEI 41–17, where the joint nonlinear behavior is calibrated using representative test results by Shiohara et al. (2013). Major differences between Option 1 and 2 joint models were in their ductility

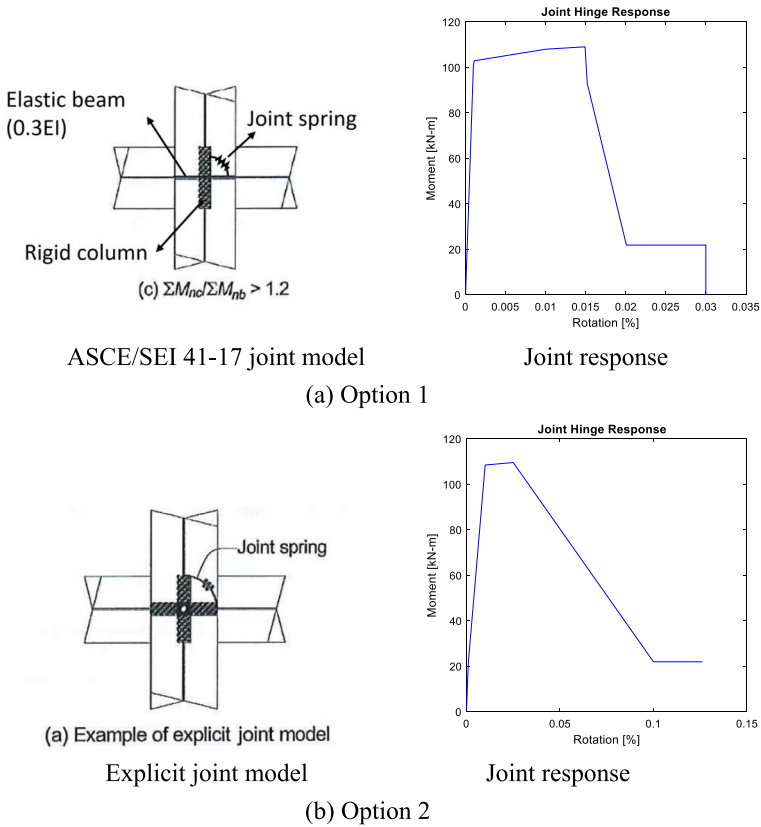


Fig. 3 Modeling of beam-column joints in OpenSees NJ model

and the abruptness of strength degradation, where Option 1 model (ASCE-41 compliant) had considerably less ductility and more abrupt strength degradation, as illustrated in Fig. 3a. For both options, the hysteresis behavior was modeled using the Pinching4 hysteretic model in OpenSees.

It should be noted that nonlinear joint behavior was only modeled for the perimeter frames over floors 1 to 7 because: (1) preliminary analyses indicated limited or no nonlinearity at levels 8 to 10 and (2) results of a pushover analysis for a lateral load distribution based on a first mode shape, indicated that the interior frames (beams connecting to wall boundary versus perimeter frames) contributed only about 23% of the total lateral strength of the building (77% for perimeter frames).

The walls were determined to respond primarily in a flexure mode based on their long height-to-length aspect ratio and high shear strength to shear demand ratio (Unal et al., 2020). Therefore, shear behavior of the walls is modeled as essentially elastic using effective shear modulus of $0.2E_{cE}$, versus using a value of $0.4E_{cE}$, as recommended by ASCE/SEI 41–17. Since wall shear demands (and shear deformations) are low, this assumption is expected to have very little influence on the results presented later.

3.3 Material models and modeling strength degradation

For the fiber section elements, sections were discretized and assigned material models: Concrete02 for unconfined and confined concrete and wall boundary elements, and SteelMPF for reinforcing bars. Basic parameters of the stress–strain curve for unconfined and confined concrete in compression were calculated using the models proposed by Saatcioglu and Razvi (1999) and Mander et al. (1988) based on cylinder test data and the amount of transverse reinforcement provided in the cross-section. Tensile strength of concrete was taken as $0.31 \sqrt{f'_c}$ (MPa) based on Belarbi and Hsu (1994) constitutive model for concrete in tension. The tangent stiffness of concrete material at zero load was defined as $2f'_c/\epsilon_0$ and the degrading slope E_t was defined as 5% of the tangent stiffness of concrete material at zero load. Reinforcement stress–strain relations were based on direct tension tests of reinforcement coupons.

Material models calibrated based on as-tested material properties were further modified in plastic hinge regions of walls, beams, and columns to capture strength degradation in these elements according to ASCE/SEI 41–17. It was assumed that steel reinforcement in compression loses its capacity at the strain where concrete reaches its residual capacity (EpsU). EpsU parameter was calibrated such that strength loss occurs at plastic rotation that corresponds to ASCE/SEI 41–17 Parameter a for walls, beams, and columns. Examples of calibrated moment-rotation relationships for representative wall, beam, and column elements are presented in Fig. 4. Axial loads used in calculating ASCE/SEI 41–17 modeling parameters for joints and acceptance criteria for all structural elements were obtained as the maximum compressive axial demands developed in each element from a pushover analysis of the building out to initiation of loss of lateral load carrying capacity using a first mode lateral load distribution. Slab out-of-plane bending was not modeled explicitly but was rather accounted for through effective flange widths assigned to the beams calculated in line with ACI 318–14.

3.4 Analysis approach

The ground motions applied to the model were the recorded motions at the base of the test building (on the shake table). For the purposes of this study, the acceleration histories of the two horizontal components of the 100% JMA-Kobe record as measured at the base of the structure during the fixed-base test were used for the OpenSees models to assess the building performance. Nonlinear models were only subjected to the two horizontal

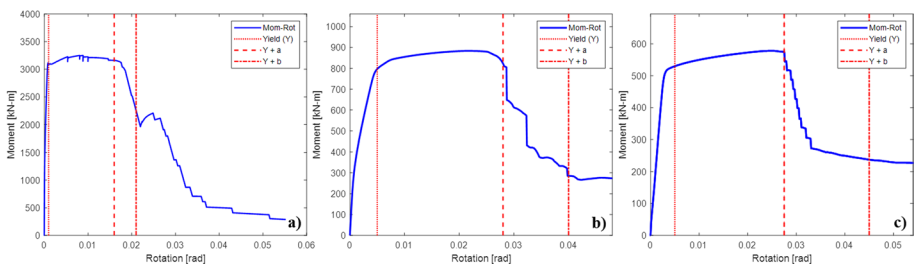


Fig. 4 Representative moment-rotation responses for calibrated section of structural elements: **a** walls, **b** columns, **c** beams

components of the JMA-Kobe 100% motion (recorded on the shake table) without being subjected to the prior motions applied to the building in the experimental program. Model results from the JMA-Kobe 100% record was used for the comparison to the observed performance because it was the first test during which severe damage and significant nonlinear response was recorded. Only minor yielding was recorded during the 50% JMA-Kobe fixed-base test and the yielding did not result in any appreciable permanent deformation (Nagae et al. 2015). The potential influence of the prior test runs (i.e., sequential application of 50% and 100% JMA-Kobe) is addressed by conducting a limited sensitivity study.

Because the building did not contain any nonstructural elements, the analysis employed 2% Rayleigh damping defined at $0.2T_j$ and $1.5T_j$. The analysis accounted for nonlinear geometry effects using the P-delta transformation.

4 Comparison of analysis results with experimental observations

Given significant nonlinearity in the joints observed in the test structure after 100% JMA-Kobe ground motion was applied, model results in this section are presented only for the NL joint models (Option 1 and Option 2). Impact of using the elastic joint model and the influence of applying sequential ground motions is presented in Sect. 5.

4.1 Natural periods

The initial periods obtained from the model are compared with values obtained from the test structure in Table 2. The computational model produces periods that are larger and smaller than measured during the test for the frame and wall directions, respectively. Note that initial stiffness of the model is calculated after application of gravity load. The higher model period for the frame direction may be due to the modeling of joint flexibility per ASCE 41, which assumes zero rigid offset for the relatively short span beams (Sect. 3.2, Fig. 3a). In the wall direction, the lower model period may be due to the high initial stiffness values associated with the use of uniaxial stress–strain relations, whereas temperature and shrinkage cracking, especially at the foundation–wall interface, might be expected to lead to cracking and a reduction in stiffness for the test structure. Test periods elongate substantially in the 50% and especially the 100% JMA-Kobe tests for the frame direction likely due to joint damage, whereas elongation of model periods is less pronounced in wall direction. Note that model periods obtained after application of a ground motion are obtained by conducting modal analysis after sufficient free vibration analysis time is applied. Therefore, calculated periods depend on tangent stiffness of each of the elements in the model and provide only an approximation of the building period after the application of the ground motions, which might be sensitive to the element hysteresis rules used.

4.2 Global mechanism and damage distribution

Damage distribution data are compared against experimental measurements and observations to assess the extent to which the OpenSees models were capable of capturing the overall building deformation mechanisms and damage distribution.

Damage distribution for the frame direction for the JMA Kobe 100% record are presented in Fig. 5 for OpenSees NJ Option 1 and Option 2. Figure 5 also illustrates example joint and column hysteresis relations for the two joint modeling options. The level of

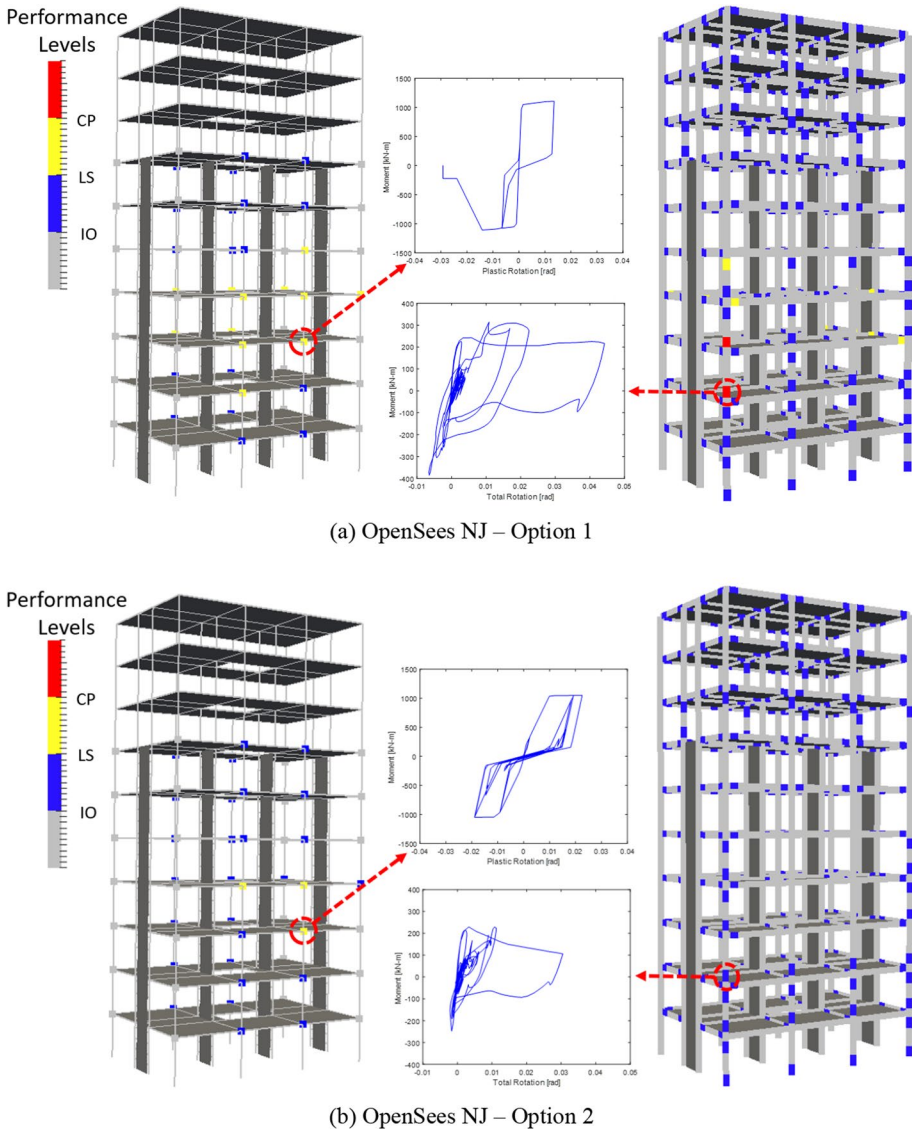


Fig. 5 OpenSees NJ: Schematic damage distribution in frame joints (left) and beams/columns (right) based on estimated plastic rotation compared to ASCE/SEI 41–17 performance levels (IO, LS, CP) (JMA Kobe 100%)

damage from analysis was obtained by comparing the inelastic rotations of beams, columns, and beam-column joints with the ASCE/SEI 41–17 performance levels (IO, LS, and CP). If the rotation of a component exceeded its LS value, then that structural component was considered to have sustained severe damage per the analysis; otherwise, it was classified as only having moderate damage. For beams and columns, the computational rotations were obtained by integrating curvatures over the length (or height) of the first element, generally set at one-member depth. The IO, LS and CP values determined for

the conforming joints from Table 10–11 of ASCE/SEI 41–17 were 0.0, 0.02 and 0.03 for the interior joints and 0.0, 0.015 and 0.02 for the exterior joints, respectively. For beams, modeling parameters and acceptance criteria were obtained from Table 10–7 of ASCE/SEI 41–17 for flexure-controlled beams with conforming transverse reinforcement and were in the range of 0.005–0.01 (IO), 0.02–0.025 (LS and Parameter a), and 0.03–0.05 (CP and Parameter b). Similarly, modeling parameters and acceptance criteria for columns were derived from Table 10–8 of ASCE/SEI 41–17 assuming that columns are not controlled by inadequate development or splicing of longitudinal reinforcement, and were in the range of 0.002–0.005 (IO, $0.15 \times a$ parameter), 0.017–0.032 (LS, $0.5 \times b$ parameter), and 0.024–0.044 (CP, $0.7 \times b$ parameter).

As can be observed in Fig. 5, for the NJ model with Option 1 joint modeling parameters, about half of the joints exceed the IO or LS performance level. Results obtained for Option 2 joint model are similar, with smaller amount of nonlinearity in the joints, where only three interior joints exceed the LS performance level. Results indicate that most interior joints at floors 3 and 4 exceeded the LS parameter for joint model Option 1, with modestly lower ratios for joint model Option 2, as expected. This suggests that severe damage would occur at these joints. However, comparison of joint plastic rotation with ASCE/SEI 41–17 performance levels suggests that none of the joints exceeded the collapse prevention rotation limit for both Option 1 and Option 2 models. The model results suggest no damage would be observed in the exterior joints. This is consistent with what was observed in the test (Fig. 6) where severe damage was observed for interior joints at the 3rd and 4th floors and modest damage was observed for interior joints at the 2nd and 5th floors.

As indicated in Fig. 5, for both joint modeling options, beams primarily remained elastic. For Option 2, all beams are within the IO performance level, while for Option 1 model only a few beams experienced plastic rotations that exceeded LS performance level. Peak column plastic rotation demands computed from the models were generally within IO performance level, with higher ratios for joint model Option 1 (particularly for exterior (corner) columns), as would be expected. For Option 2, all columns are within the IO performance level, while for Option 1 only few column sections experienced plastic deformations that exceed LS and CP performance levels, while the vast majority of the remaining columns are within the IO performance level. It can be concluded based on results presented in Fig. 5 that only minor lateral strength degradation is predicted using NJ model Option 1, where column rotations exceed the CP acceptance limit for only one column, while NJ model Option 2 does not predict any strength degradation, which is consistent with experimental observations (Tosauchi et al. 2017).

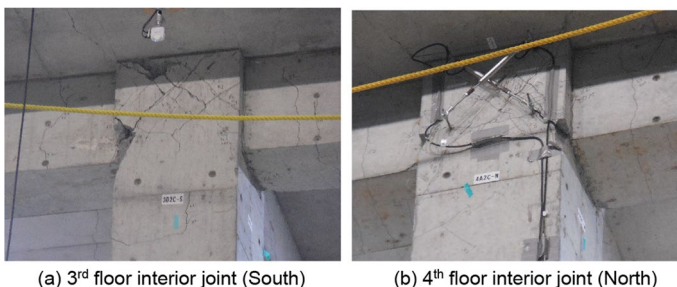


Fig. 6 Observed joint damage after application of JMA Kobe 100% (fixed-base)

It should be noted that column yielding is observed in the model despite column-to-beam moment strength ratios exceeding the 1.2 value required by ACI 318–14 Sect. 18.7.3 (i.e., strong column-weak beam requirement). Column yielding occurred because: (1) higher modes and nonlinear responses produce higher beam moment and shear demands than predicted by ASCE/SEI 7 (Moehle 2015; NIST GCR 16–917-40, Sects. 3.1 and 5.5.3), and (2) the approach commonly used to determine column moments at a beam-to-column connection is approximate (e.g., see ACI PRC 352–02; NIST GCR 16–917-40). It is also noted the modeling parameters were computed for maximum compression axial load determined from a pushover analysis using the first mode lateral load distribution, whereas column yielding generally occurred during the analysis at minimum axial load; therefore, the reported ratios for columns are likely on the conservative side.

Estimated plastic rotation demands for the wall direction are presented in Fig. 7a and were determined to be less than $0.5a$ and $0.25b$ for ASCE/SEI 41–17, i.e., wall deformation demands are within IO performance level. The results indicated limited yielding at the base of the wall, which is consistent with the observed modest cracking and very limited spalling at the wall boundaries (Fig. 7b, c).

4.3 Base shear and roof displacement (drift)

Base shear was derived from the test results using acceleration computed at the center of mass (COM) of the test structure multiplied by the floor mass for each level, summed over the ten floors. The roof drift ratio is defined as the roof lateral displacement with respect to the foundation divided by the total building height (25.75 m=84.48 ft) from the base of the 1st story columns to the roof level. The history of the roof drift versus base shear for the test and model are shown in Fig. 8 for the frame and wall directions for the JMA Kobe 100% motion. In general, results obtained using Option 1 and Option 2 models were very similar and match reasonably well the experimental data, with overall slightly better match for joint model Option 2. Therefore, due to space limitations, results are presented only for Option 2 model.

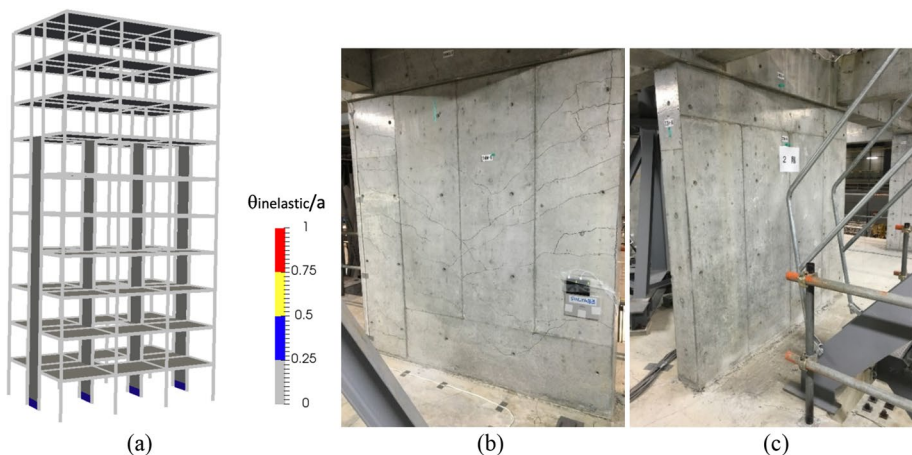


Fig. 7 Predicted and observed damage distribution in walls (JMA Kobe 100%): a) schematic damage distribution within wall obtained using NDP OpenSees NJ compared to ASCE/SEI 41–17 plastic rotation parameter “a”, b) wall damage at 1st floor, c) wall damage at 2nd floor

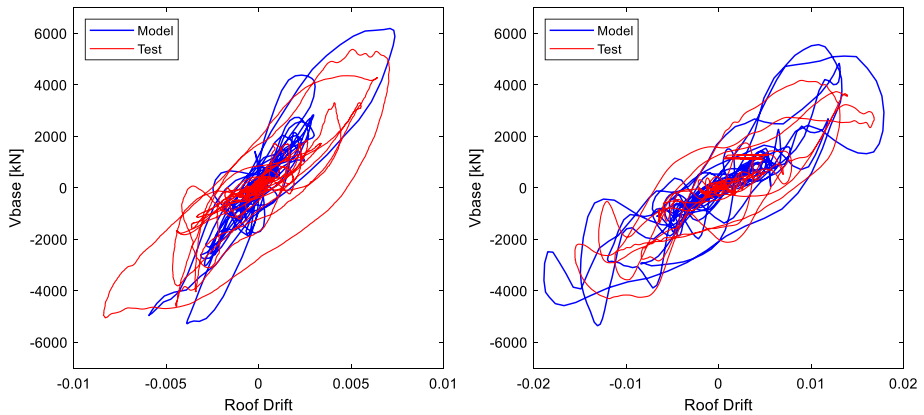


Fig. 8 OpenSees NJ—Option 2: Roof drift versus base shear histories for JMA-Kobe 100%—Wall direction (left), Frame direction (right)

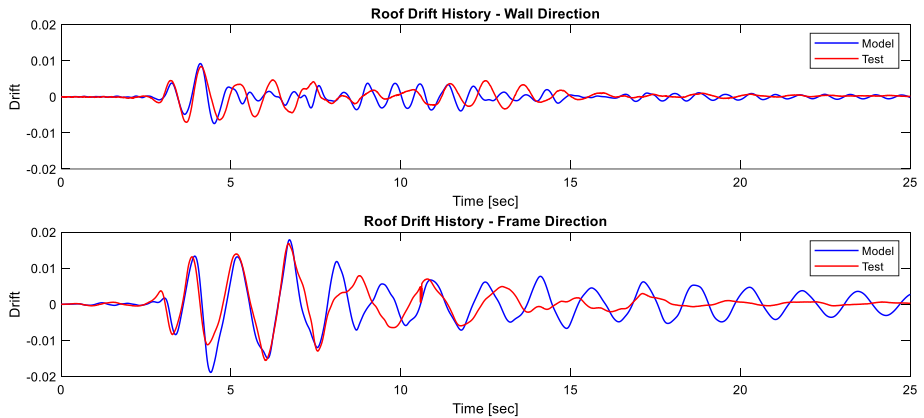


Fig. 9 OpenSees NJ—Option 2: Roof drift histories for JMA-Kobe 100% —Wall direction (top), Frame direction (bottom)

The roof drift histories for test structure at COM and the OpenSees model are plotted in Fig. 9 for the JMA Kobe 100% motion. The results indicate that the histories, especially the peak values, show similar tendencies. The only notable discrepancy between the model and test results can be observed at about 4.5 s in the frame direction, where model overestimates the roof drift by approximately 80%. Fundamental periods for the model appear to be slightly low and high relative to the test building for the wall and frame directions, respectively. The model does appear to show higher peak drifts later in the history, possibly due to contributions from higher modes and variations in damping (e.g., foundation level damping); however, peak values are well captured.

Base shear histories are plotted in Fig. 10, which demonstrates that model predicts with very good accuracy history of base shear in the wall direction, while in the frame direction maximum base shear predicted by the model (at around 4.5 s) is approximately 20% larger than the one obtained from test data.

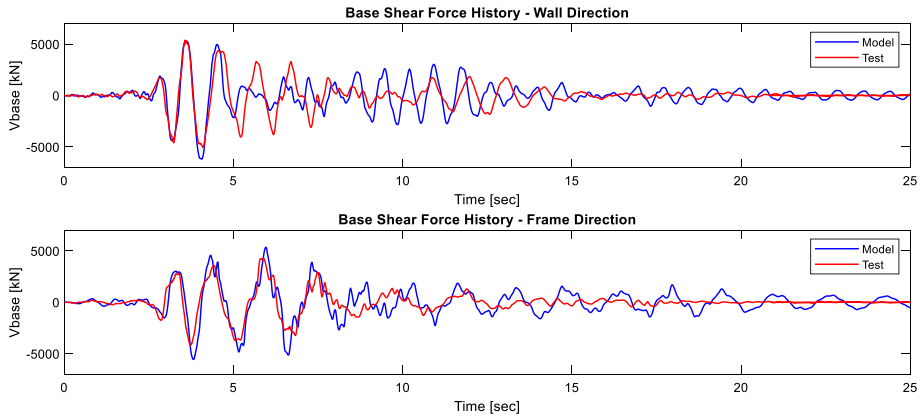


Fig. 10 OpenSees NJ: Base shear histories for JMA-Kobe 100% —Wall direction (top), Frame direction (bottom)

4.3.1 Peak story drift

Distribution of maximum story drifts over the building height are compared between the OpenSees NJ model and the test measurements in Fig. 11. Results for the wall direction agree quite closely, although test values are approximately 10% higher (on average) for the bottom 5 stories and 10% lower for the top 4 stories. Results for the frame direction show larger discrepancy between test and joint model Option 1, especially between the 2nd and 5th levels, where the model overestimates story drift by 80%. However, results for joint model Option 2 match the test results very well with mismatch between analytical and experimental results that is $\pm 5\%$. The results imply that the strength degradation for the ASCE/SEI 41–17 joint backbone relations used in Option 1 are too abrupt.

4.3.2 Residual story drift

Residual drifts are obtained from the analysis by applying sufficient free-vibration time after the application of the 100% JMA-Kobe ground motion to allow model of the structure to come to rest. Residual story drifts over the building height are plotted in Fig. 12 for joint model Option 2 (results for joint model Option 1 are similar) and are relatively small, i.e., less than 0.001 for all stories.

4.3.3 Peak floor accelerations

Figure 13 compares the peak floor accelerations from the NJ model and measured in the experiment and indicates reasonable agreement in the acceleration profiles at all levels for both the wall and frame directions, although model results tend to systematically overestimate peak floor accelerations by approximately 1.5 to 2.0 times, especially in the frame direction. This may be related to damping assumptions used in the analysis.

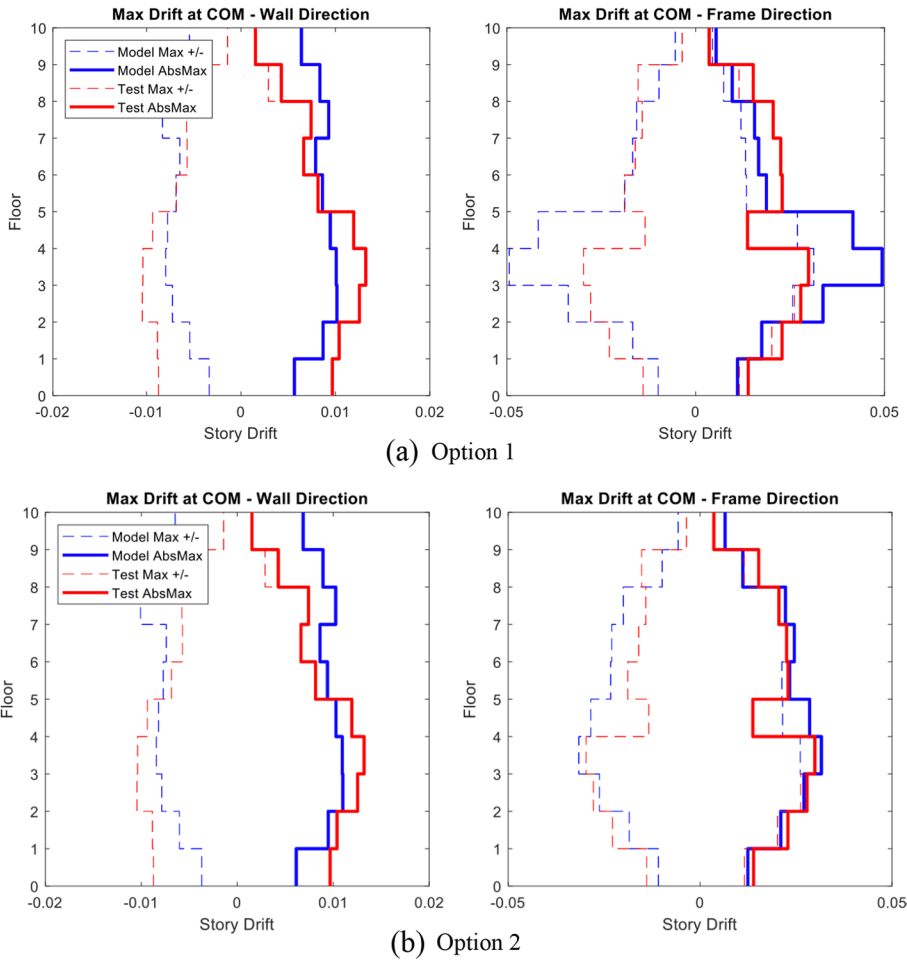


Fig. 11 OpenSees NJ: Peak story drift ratios for JMA-Kobe 100% —Wall direction (left), Frame direction (right)

5 Sensitivity studies

5.1 Elastic joint modeling

The OpenSees NJ model was modified to have elastic joint elements, which are not allowed to yield or lose strength (OpenSees EJ model). This is a common modeling approach in engineering practice. Considering the noted premature joint strength loss that occurred in the OpenSees NJ model Option 1 (ASCE/SEI 41–17 compliant model), this OpenSees EJ model is considered to investigate the effects of joint nonlinearity on demands in adjacent members and to compare test and model results.

Figure 14 shows the damage distribution in terms of plastic rotations ($\theta_{inelastic}$) derived from the computational OpenSees EJ model and compares the results with the one obtained using OpenSees NJ model Option 1. The wall direction damage distribution is almost identical for this model as for the OpenSees NJ model. In the frame

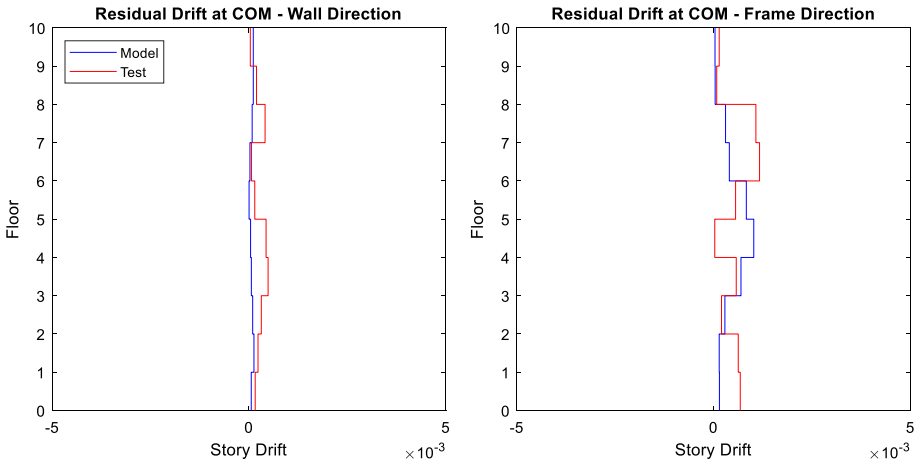


Fig. 12 OpenSees NJ—Option 2: Peak residual story drifts for JMA-Kobe 100% —Wall direction (left), Frame direction (right)

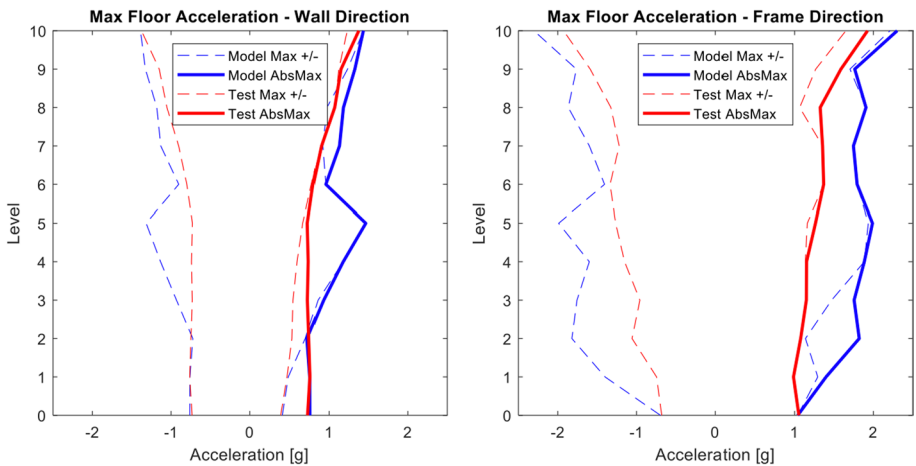


Fig. 13 OpenSees NJ—Option 2: Peak floor accelerations for JMA-Kobe 100% —Wall direction (left), Frame direction (right)

direction, the 3rd story columns are more severely damaged in the OpenSees model with elastic joints (EJ) than in the OpenSees nonlinear joint (NJ) model, that is, the peak column plastic rotation approximately doubles for the 3rd story columns. When nonlinear joints are used, the damage concentrates in the joints which unloads the beams and columns as seen in the OpenSees NJ model. When joints are prevented from losing strength (i.e., modeled elastically), the damage concentrates more in the column than the beams.

The distribution of maximum floor accelerations over the building height are compared for the OpenSees NJ Option 1 and EJ models in Fig. 15. The comparison reveals that joint yielding reduces the floor accelerations over the stories where joint damage

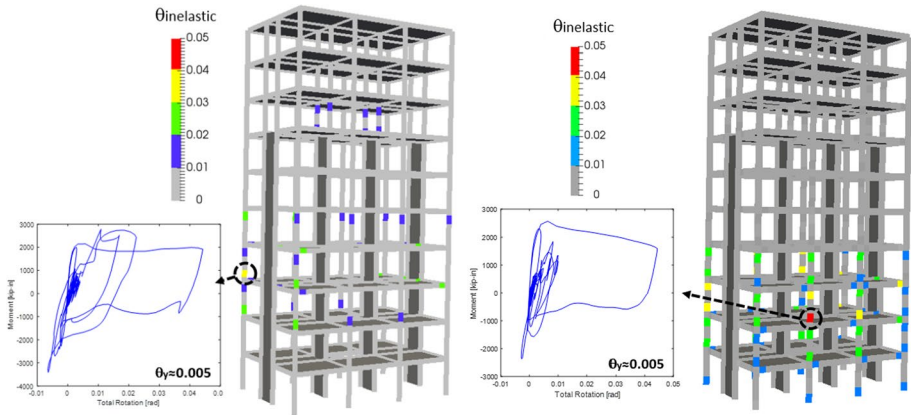


Fig. 14 Schematic damage distribution in columns for NJ model Option 1(left) and EJ columns (right) for JMA Kobe 100%

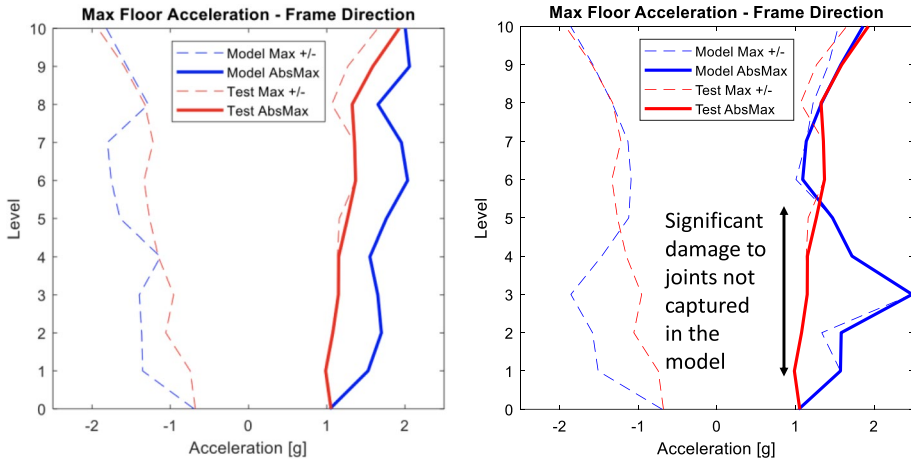


Fig. 15 Maximum floor acceleration comparison for OpenSees NJ Option 1(left) and EJ (right) models throughout the height of the building for JMA-Kobe 100%

was observed (3rd to 5th floors), and most notably, at 3rd floor. However, the NJ models consistently over predict peak floor accelerations at all floors.

The distribution of maximum story drifts over the building height are compared between the OpenSees NJ (Option 1) and EJ models and experiment in Fig. 16. Joint modeling did not alter the wall direction drift results measurably, and thus they are not presented. For the frame direction, drifts predicted with the EJ model were significantly smaller at 4th and 5th level and modestly smaller elsewhere, except the 2nd and 3rd level, comparing to the results of NJ model; the reductions at levels 3 through 5 were likely because of damage concentration at these levels for both the NJ model (in the joints) and EJ model (in the columns).

Findings from comparing the OpenSees NJ and EJ models highlight the importance of considering and modeling all sources of nonlinearity and also using accurate modeling

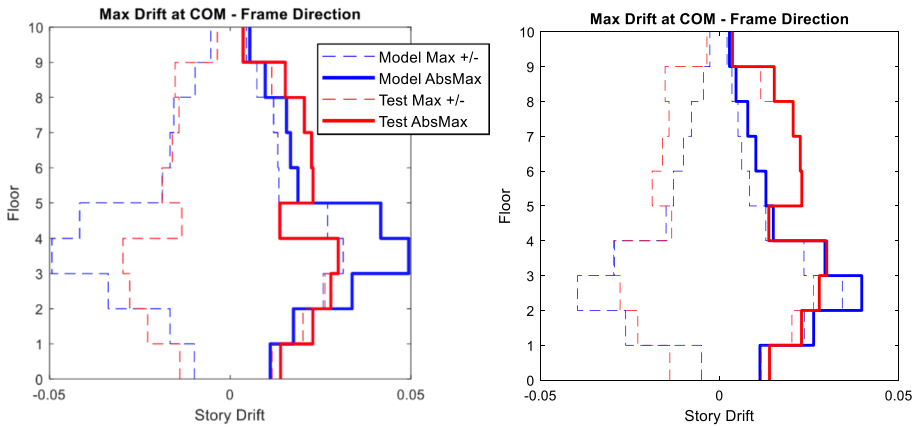


Fig. 16 OpenSees: Maximum story drift comparison for OpenSees NJ Option 1 (left) and EJ (right) models throughout the height of the building for JMA-Kobe 100%

parameters (e.g., rate of strength degradation) in nonlinear analysis to avoid skewing building demands, component demands, and damage distributions. The results also indicate that joint yielding may occur even if ASCE/SEI 41 mechanism analysis indicates joint shear strength is not exceeded because of differences in the assumptions used for the mechanism analysis and the demands from the nonlinear dynamic response history analysis.

5.2 Sequential application of ground motions

Ground motions for JMA Kobe 50% and 100% were applied sequentially to the model to assess the potential influence of the repeated motions on the comparisons of model and test results for peak story drifts and peak story accelerations. The analysis of the 50% Kobe ground motion revealed that minor yielding occurred in beam column joints at 2nd, 3rd, and 4th floor, where maximum plastic rotations in the joints were less than 1.0%, while beams, columns, and walls remained essentially elastic. These analytical results are in line with experimental observations after the application of the 50% Kobe ground motion (Tosauchi et al 2017). Yielding of the beam-column joints during 50% Kobe ground motion softened the analytical model before the application of the 100% Kobe ground motion and increased its fundamental period in the frame direction from initial 0.67 s to 1.14 s. For wall direction, the change in fundamental period was much less pronounced, where period increased from 0.43 s to only 0.57 s likely due to wall cracking (no yielding was observed). Softening of the analytical model, particularly in the frame direction, is the primary reason for notable effect of application of consecutive ground motions described in this section.

Results presented in Fig. 17 through Fig. 20 indicate that the maximum story drifts are modestly impacted and produce a better match between model and test results for the frame direction at all levels and for the wall direction at lower levels (Figs. 18, 19, 20). Maximum floor accelerations do not change significantly. Note that analysis results for the frame direction (Fig. 19) indicate that maximum drifts (stories 3–5) are smaller when sequential ground motions are applied, which might seem counterintuitive. However, detailed investigation of analysis results showed that 50% Kobe ground motion applied first to the model changed the dynamic properties of the building by

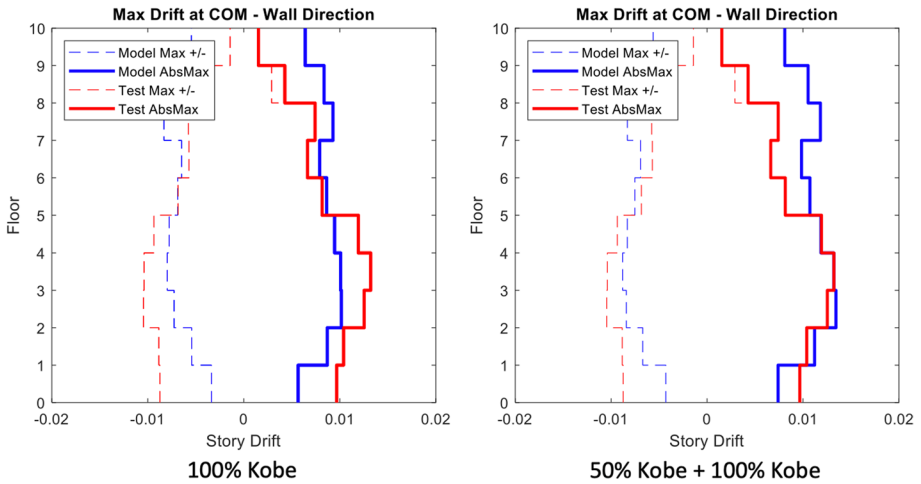


Fig. 17 OpenSees NJ Option1: Peak story drift ratios for Wall direction for JMA Kobe 100% (left), JMA Kobe 50% + 100% direction (right)

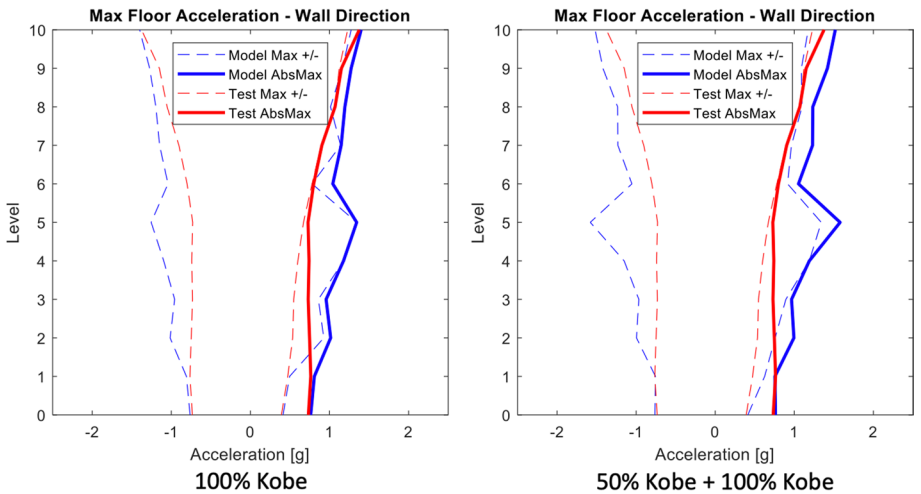


Fig. 18 OpenSees NJ Option1: Peak floor accelerations for Wall direction for JMA Kobe 100% (left), JMA Kobe 50% + 100% direction (right)

making the structure softer such that drifts experienced by the model during subsequent 100% Kobe ground motion are smaller compared to drifts obtained from analysis conducted by applying only 100% Kobe ground motion (this observation is also a result of the spectral shape). This result was not observed for the wall direction, likely due to the limited nonlinear curvature demands at the wall base in the 50% Kobe test (essentially linear wall response).

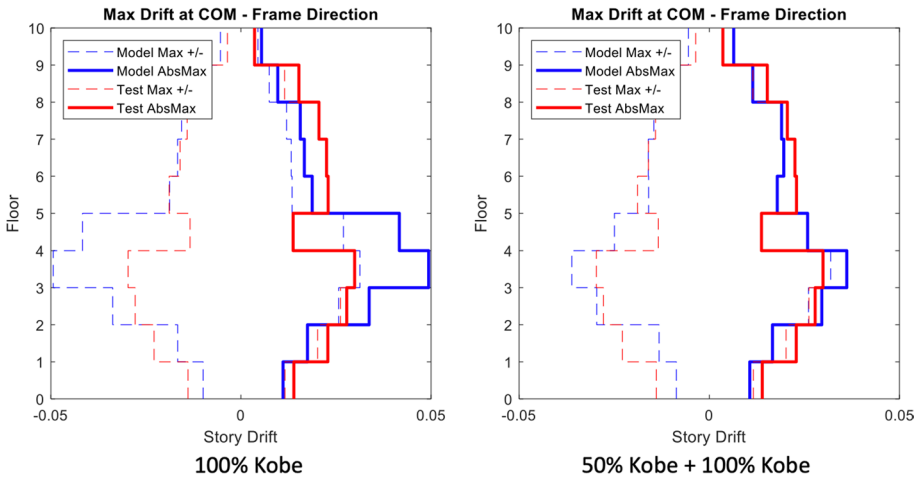


Fig. 19 OpenSees NJ Option1: Peak story drift ratios for Frame direction for JMA Kobe 100% (left), JMA Kobe 50% + 100% direction (right)

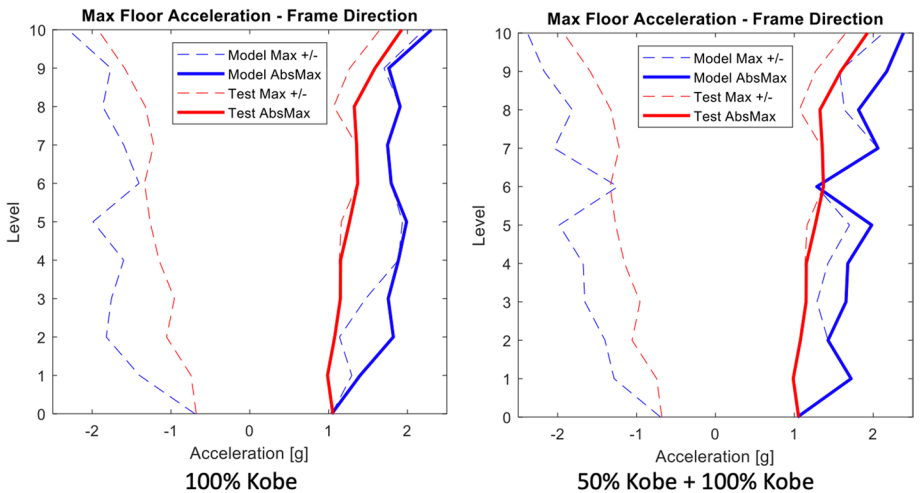


Fig. 20 OpenSees NJ Option1: Peak floor accelerations for Frame direction for JMA Kobe 100% (left), JMA Kobe 50% + 100% direction (right)

6 Summary and conclusions

This paper presents results of an analytical benchmark study conducted for a 10-story RC building tested at the E-Defense shake table in December 2015. Analytical model is generated in OpenSees software following ASCE/SEI 41–17 nonlinear dynamic evaluation procedures. Analysis results were obtained using 100% JMA-Kobe ground motion and compared with global and local experimental measurements and observed damage distribution to judge the effectiveness of the ASCE/SEI 41–17 provisions.

The ASCE/SEI 41–17 nonlinear dynamic evaluation procedures were overall able to reasonably identify the general damage extent and distribution for the frame direction. Good agreement was observed for roof drift histories (except later in the history) and for peak roof drifts. Base shear was not as well predicted, possibly due to variations in the contributions of higher modes and the foundation flexibility.

The distribution of damage between various components in the frames (beams, columns, joints) varied significantly depending on the modeling approach. Modeling nonlinear joint behavior led to improved correlations, especially for joint model Option 2, with more gradual joint strength degradation. For the OpenSees NJ models, damage tended to concentrate within interior joints (more so for Option 1), which led to smaller nonlinear deformations in beams and columns.

For the wall direction, the damage location and severity at the base of the walls was captured well by nonlinear models constructed according to ASCE/SEI 41–17 requirements. However, the plastic rotation demands imposed on the walls were modest, only reaching 25% to 50% of the ASCE/SEI 41–17 parameter a (strength loss). Therefore, the light damage observed (very minor concrete spalling at extreme edge of wall) appears consistent with the computed demands.

This study highlights the effects of having modeling parameters with varying degrees of conservatism (or accuracy) in ASCE/SEI 41–17. In the frame direction, modeling of nonlinear joint behavior was important to produce improved comparisons between test and model results, as nonlinear joint responses relieved deformation demands on the beams and columns. The EJ models prevented joints from yielding and degrading (stiffness and strength), resulting in higher demands (damage) on adjacent beams and columns. Each of these scenarios would therefore result in different retrofit outcomes for the building and highlight the importance to ensure that ASCE/SEI 41 nonlinear modeling parameters for all elements target consistent mean estimates from experimental data, such that building response is not artificially skewed. Results for the NJ models highlighted the importance of modeling nonlinear joint behavior, with results for the OpenSees model for ASCE/SEI 41–17 indicating damage would concentrate within the interior joints as observed in the tests. The results from the OpenSees models suggested that the beam-column joint modeling parameters in ASCE/SEI 41–17 for nonlinear dynamic procedures likely over-estimate the rate of strength loss with increasing demands. A review and update of the joint shear strength and nonlinear modeling parameters and acceptance criteria in ASCE/SEI 41–17 may be justified for future study. For the wall direction, all models produced acceptable results for roof drift, story drifts, and floor accelerations, likely due to the simplicity of the structural system (lightly coupled, cantilever walls) and the limited nonlinear demands. The damage at the base of the walls during the experiment was relatively minor and was consistent with the analysis results from both Open Sees.

Because the test structure was subjected to many different intensity runs, comparisons of test and model periods are somewhat complicated. For the OpenSees models, initial periods (initial tangent) are 0.67 and 0.43 s for the frame and wall directions, respectively, whereas test structure periods were 0.57 s for both the frame and wall directions. ASCE/SEI 41–17 stipulates that all the members in buildings should be modeled using stiffness values corresponding to secant to yield. In the test building, not all members reach yield level demands, particularly at higher floor levels and the test building was subjected to prior motions that induced cracking and stiffness reductions. Similar issues exist for real buildings. In this study, peak roof level and story drifts were reasonably well predicted with model results, although results for the more sophisticated OpenSees models generally produced closer predictions to the measured results, suggesting that using stiffness values

that vary with demand level (i.e., fiber models) and with prior events is likely to yield more accurate comparisons. Additional studies that address this issue and whether the costs associated with the added model complexity and computer run time are worth these added costs might be useful.

Overall, the analyses of the 10-story E-Defense test structure indicate important needs to improve modeling capabilities. These include modeling strategies to capture joint behavior and the need to base modeling parameters for all elements to their mean estimates based on experimental data such that model response and damage distributions are not artificially skewed.

Acknowledgements This study was funded by NIST Contract No. 1333ND19PNB730832 under the ATC-134-1 project. The authors would like to thank to all contributing members of the ATC-134-1 project, especially Russell Berkowitz and Dustin Cook for their valuable feedback. Any opinions, findings, and conclusions expressed herein are those of the authors and do not necessarily reflect those of the sponsors.

Author contributions All authors contributed to the study conception and design. The modeling and analysis were performed by KK and SA in collaboration with John Wallace. The test and data collection were performed by KK. The first draft of the manuscript was written by KK, SA and JW. All authors commented on previous versions of the manuscript. All authors read and approved the final manuscript.

Funding This work was supported by funding from National Institute of Standards and Technology (Grant No. 1333ND19PNB730832) awarded to Prof. John Wallace and UCLA.

Data availability The datasets generated during and/or analyzed during the current study are available from the corresponding author on reasonable request.

Declarations

Conflict of interests The authors have no relevant financial or non-financial interests to disclose.

References

- ACI (2014) Building code requirements for structural concrete and commentary, ACI 318–14. American Concrete Institute, Farmington Hills, Michigan
- ACI (2017) Standard requirements for seismic evaluation and retrofit of existing concrete buildings and commentary, ACI CODE-369.1-17. American Concrete Institute, Farmington Hills Michigan
- Architectural Institute of Japan. (2018) Design guidelines for earthquake resistant reinforced concrete
- ASCE, SEI 41 (2017) Seismic evaluation and retrofit of existing buildings (ASCE/SEI 41–17). American Society of Civil Engineers, Virginia
- ASCE, SEI 7–16 (2017) Minimum design loads and associated criteria for buildings and other structures. American Society of Civil Engineers, Virginia
- Belarbi A, Hsu TC (1994) Constitutive laws of concrete in tension and reinforcing bars stiffened by concrete. *ACI Struct J* 91(4):465–474
- Buniya M, Simpson B, Macedo J, Vargaray L, Barbosa A (2020) Collapse fragility function development using conditional scenario spectra: application to a multi-story reinforced concrete shear wall. In: Proceedings of 17th World Conference on Earthquake Engineering, 17WCEE, Sendai, Japan - September 13th to 18th 2020
- Celik OC, Ellingwood BR (2008) Modeling beam-column joints in fragility assessment of gravity load designed reinforced concrete frames. *J Earthquake Eng* 12(3):357–381
- Computers and Inc. Structures (2018) PERFORM 3D, user guide v4, non-linear analysis and performance assessment for 3D structures. Computers and Structures, Inc., Berkeley, CA
- Garcia Gomez CA (2020) “Nonlinear dynamic analysis of a ten-story reinforced concrete building.”, MS Thesis, University of California, Los Angeles, Department of Civil & Environmental Engineering, pp: 60

- Kajiwara K, Tosauchi Y, Sato E, et al (2015) Three-dimensional shaking table test of a 10-story reinforced concrete building on the E-Defense, part1: overview and specimen design of the base slip and base fixed tests". In: 16th world conference on earthquake, 16WCEE 4012 (2017)
- Kolozvari K, Anaraki K, Orakcal K, Wallace JW (2021) "Three-dimensional model for nonlinear analysis of slender flanged reinforced concrete walls. *Eng Struct* 236(112105):1–17. <https://doi.org/10.1016/j.engstruct.2021.112105>
- Mander JB, Priestley MJ, Park R (1988) Theoretical stress-strain model for confined concrete. *J Struct Eng* 114(8):1804–1826
- McKenna F (2011) OpenSEES: a framework for earthquake engineering simulation. *Comput Sci Eng* 13(4):58–66
- Moehle J (2015) Seismic design of reinforced concrete buildings. McGraw-Hill education, Vol. 31. McGraw-Hill Education. <https://www.accessengineeringlibrary.com/content/book/9780071839440>
- Nagae T, Ghannoum WM, Kwon J, Tahara K, Fukuyama K, Matsumori T, Shiohara H, Kabeyasawa T, Kono S, Nishiyama M (2015) Design implications of large-scale shake-table test on four-story reinforced concrete building. *ACI Struct J* 112(2):135
- NIST, 2009, Research Required to Support Full Implementation of Performance-Based Seismic Design, NIST GCR 09–917–02, prepared by the Building Seismic Safety Council of the National Institute of Building Sciences for the National Institute of Standards and Technology, Gaithersburg, Maryland.
- NIST, 2022, Benchmarking evaluation methodologies for existing reinforced concrete buildings, NIST GCR 22–917–50, prepared by applied technology council. <https://doi.org/10.6028/NIST.GCR.22-917-50>
- Razvi S, Saatcioglu M (1999) Confinement model for high strength concrete. *J Struct Eng ASCE* 125(3):281–289
- Sato E, Tosauchi Y, Fukuyama K, et al. (2015) Three-dimensional shaking table test of a 10-story reinforced concrete building on the E-Defense, Part2: specimen fabrication and construction, test procedure, and instrumentation program". In: 16th world conference on earthquake, 16WCEE 4007 (2017)
- Shiohara H, Sho H, Kusahara F, 2013, "Behavior at large deformation of R/C interior beam-column joints of joint yielding," Summaries of Technical Papers of Annual Meeting, Architectural Institute of Japan, pp. 723–724. (In Japanese)
- Sattar S (2018) Evaluating the consistency between prescriptive and performance-based seismic design approaches for reinforced concrete moment frame buildings. *Eng Struct* 174:919–931
- Tosauchi Y, Sato E, Fukuyama K, et al. (2015) Three-dimensional shaking table test of a 10-story reinforced concrete building on the E-Defense, Part3: base slip and base fixed test results". In: 16th world conference on earthquake, 16WCEE 4016 (2017)
- Unal ME, Kolozvari K, Wallace JW, Kajiwara K, Kang J-D, Tosauchi Y, Sata E, Kabeyasawa T, Shiohara H, Nagae T, Kabeyasawa T, (2020) Assessment of the 2015 and 2018 E-defense 10-story reinforced concrete buildings based on ACI 318–19 and ASCE/SEI 7–16, Draft final report, UCLA structural/ earthquake engineering research laboratory report SEERL 2020/2

Publisher's Note Springer Nature remains neutral with regard to jurisdictional claims in published maps and institutional affiliations.

Springer Nature or its licensor (e.g. a society or other partner) holds exclusive rights to this article under a publishing agreement with the author(s) or other rightsholder(s); author self-archiving of the accepted manuscript version of this article is solely governed by the terms of such publishing agreement and applicable law.